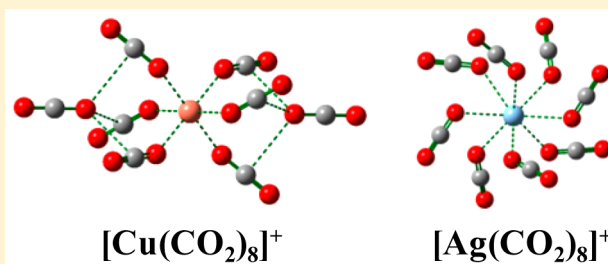


Reactions of Copper and Silver Cations with Carbon Dioxide: An Infrared Photodissociation Spectroscopic and Theoretical Study

Zhi Zhao,^{†,‡,||} Xiangtao Kong,^{‡,§,||} Dong Yang,^{‡,§} Qinqin Yuan,^{‡,§} Hua Xie,[‡] Hongjun Fan,[‡] Jijun Zhao,^{†,||} and Ling Jiang^{*:‡,||}[†]Key Laboratory of Materials Modification by Laser, Ion, and Electron Beams, Dalian University of Technology, Ministry of Education, Dalian 116024, China[‡]State Key Laboratory of Molecular Reaction Dynamics, Collaborative Innovation Center of Chemistry for Energy and Materials (iChEM), Dalian Institute of Chemical Physics, Chinese Academy of Sciences, 457 Zhongshan Road, Dalian 116023, China[§]University of Chinese Academy of Sciences, 19A Yuquan Road, Beijing 100049, China

Supporting Information

ABSTRACT: The reaction of copper and silver cations with carbon dioxide was studied by mass-selected infrared photodissociation spectroscopy. Quantum chemical calculations were performed on these products, which aided the experimental assignments of the infrared spectra and helped to elucidate the geometrical and electronic structures. The Cu⁺ and Ag⁺ cations bind to an oxygen atom of CO₂ in an end-on configuration via a charge-quadrupole electrostatic interaction in the [M(CO₂)_n]⁺ complexes. The formation of oxide-carbonyl and carbonyl-carbonate structures is not favored for the interaction of CO₂ with Cu⁺ and Ag⁺. For $n = 3$ and 4 , the $n + 0$ structure is preferred. [Note on the nomenclature: Using $i + j$, i denotes the number of CO₂ molecules in the first coordination shell, and j denotes the number of CO₂ molecules in the second coordination shell.] The two nearly energy-identical $n + 0$ and $(n - 1) + 1$ structures coexist in $n = 5$ and 6 . While the six-coordinated structure is favored for [Cu(CO₂)_{n=7,8}]⁺, the $n + 0$ configuration is dominated in [Ag(CO₂)_{n=7,8}]⁺. The reaction of CO₂ with the cationic metal atoms has been compared to that with the neutral and anionic metal atoms, which would have important implications for understanding the interaction of CO₂ with reduction catalysts and rationally designing catalysts for CO₂ reduction based on cost-effective transition metals.



1. INTRODUCTION

The study of the interaction of carbon dioxide with metals is of considerable interest because CO₂ is a double-faced gas as an abundant renewable resource for the production of fine chemicals and clean fuels and a main contributor to global warming.^{1–3} Metal-catalyzed activation of carbon dioxide has many potential incentives with economical and environmental benefits. Extensive efforts have been made to recycle CO₂ from industrial emission and to remove some of this greenhouse gas. Transition metal catalysts have been widely used in such processes. The molecular-level understanding of a chemical reaction on a catalyst is difficult to be elucidated from the condensed phase measurement because of its complexity and the concomitant of in situ-measurements. Cluster spectroscopy coupled with mass spectrometry affords a model study for the elemental reactions on the most active or least coordinated site of a catalyst, which provides detailed structural and energetic information for mechanistic understanding of a chemical reaction.^{4–7}

The interaction of carbon dioxide with neutral, cationic, and anionic metal atoms has been investigated in the gas phase and a series of metal–CO₂ complexes have been experimentally

characterized.^{8–10} Quantum chemical calculations have been performed to understand the electronic structures and bonding characteristics of these complexes. In neutral complexes containing a single metal atom, monodentate coordination M(η^1 -CO₂) or bidentate coordination M(η^2 -CO₂) are most common. The inserted OMCO species has also been observed for all the neutral first-row transition metal atoms except Cu and Zn.^{8,11,12} In the reactions of CO₂ with metal cations, the metal cations bind to an oxygen atom of CO₂ in an end-on configuration via a charge-quadrupole electrostatic interaction.⁹ In particular, the formation of [OMCO(CO₂)_{n-1}]⁺ oxide-carbonyl species has been observed for Ti⁺, Ni⁺, and Si⁺,^{13–15} and the [V(C₂O₄)(CO₂)_{n-2}]⁺ oxalate-type species appears at $n = 7$.¹⁶ Metalloformate structure [M(η^1 -CO₂)]⁻ has been identified for Cu⁻, Ag⁻, Au⁻, and Bi⁻ anions^{17–20} and the bidentate configuration [M(η^2 -CO₂)]⁻ for Co⁻ and Ni⁻.^{21,22} The transition of metalloformate to oxalate complexes has been evidenced for Bi⁻ with increasing cluster size.²⁰ A bidentate

Received: February 10, 2017

Revised: April 7, 2017

Published: April 18, 2017



double oxygen metal–CO₂ coordination fashion has been formed in the [ClMg(η^2 -O₂C)]⁻ complex.²³ Here, we report a study on the reactions of copper and silver cations with carbon dioxide. Infrared photodissociation spectroscopy coupled with quantum chemical calculation was used to establish the structural evolution of the [M(CO₂)_n]⁺ (M = Cu, Ag) complexes.

2. EXPERIMENTAL METHOD

The experiments were carried out using a homemade infrared photodissociation apparatus, including a laser vaporization supersonic cluster source, a tandem time-of-flight (TOF) mass spectrometer, and a tunable infrared laser source.²⁴ The experimental setup has been previously described in detail. Briefly, a 532 nm laser beam from a Nd:YAG laser was focused to vaporize the rotating metal rod. The surface of the rod was polished prior to experiments to ensure a clean vaporization target. The [M(CO₂)_n]⁺ (M = Cu, Ag) complexes were produced by the reactions of the vaporized species with CO₂. The stagnation pressure of the reaction gas was approximately 5–8 atm and the gas was introduced into vacuum region using a pulsed General Valve (Series 9). After the supersonic expansion, the cationic complexes were skimmed into the acceleration region and analyzed using the first stage of the TOF system. The cations of interest were mass-selected and decelerated into the extraction region of a vertical second stage of the TOF system. Here, they interacted with a single pass of the IR photodissociation laser. The dissociation fragments and the remaining parent cations were analyzed using the vertical second stage of the TOF mass spectrometer. Typical spectra were recorded by scanning the infrared laser in step of 2 cm⁻¹. Infrared photodissociation spectra were acquired by monitoring the fragment ions as a function of the wavelength of tunable infrared laser.

Tunable infrared laser beam was generated by a KTP/KTA optical parametric oscillator/amplifier system (OPO/OPA, LaserVision) pumped by an injection-seeded Nd:YAG laser (Continuum Surelite EX). The system provided tunable IR output radiation from 700 to 7000 cm⁻¹ with a 7 ns pulse width. Pulse energies of 1–5 mJ/pulse were available at ~2350 cm⁻¹. The line width of the near-IR output was about 0.5 cm⁻¹. The wavelength of the OPO laser output was calibrated using a commercial wavelength meter (Bristol, 821 Pulse Laser Wavelength Meter).

3. COMPUTATIONAL METHOD

Quantum chemical calculations were performed using the Gaussian 09 program.²⁵ The B3LYP hybrid functional augmented with a dispersion correction (B3LYP-D3) was employed for the present calculations. The Wachters–Hay all-electron basis set was used for the Cu atom, the SDD ECP basis set for the Ag atom, and the 6-311+G(d,p) basis set for the C and O atoms. The integral grid used for all the DFT calculations was a pruned (99 590) grid (the “ultrafine” grid as defined by Gaussian 09). Relative energies and binding energies included zero-point vibrational energies. The stretches of CO₂ were scaled by a factor of 0.971, which was determined by the ratio of the experimental value (2349 cm⁻¹) to the B3LYP-D3 calculated one (2419 cm⁻¹) of free CO₂ molecule. The resulting stick spectra were convoluted by a Gaussian line shape function with a full width at half-maximum line width of 6 cm⁻¹ in order to account for line-broadening effects.

4. RESULTS AND DISCUSSION

A mass spectrum of the [Cu(CO₂)_n]⁺ cluster ions produced by pulsed laser vaporization of copper metal targets in a supersonic expansion of CO₂ is given in Figure 1 and that of [Ag(CO₂)_n]⁺

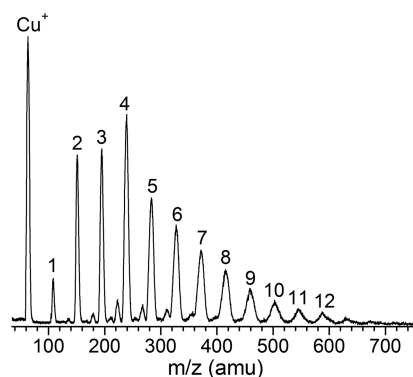


Figure 1. Mass spectrum of the [Cu(CO₂)_n]⁺ cluster ions produced by pulsed laser vaporization of copper metal targets in a supersonic expansion of CO₂.

in Figure S1. The major signals are dominated by the [M(CO₂)_n]⁺ (M = Cu, Ag; n = 1–12) clusters, which are similar to the reactions of CO₂ with Fe⁺, Co⁺, and Ni⁺.^{26–28} In contrast, the [MO(CO₂)_n]⁺ (M = Ti, V, Si) complexes were also observed in significant abundance.^{13,15,16}

These [M(CO₂)_n]⁺ (M = Cu, Ag) clusters of interest were mass-selected and introduced into the infrared photodissociation region. The selected cations can absorb photons and fragment by losing CO₂ when the IR-active vibration of the cation is resonant with the tunable infrared laser frequency. The lowest dissociation energy for the loss of one CO₂ in [Cu(CO₂)₂]⁺ is estimated to be 98.6 kJ/mol from the present calculations, indicating that assuming internally cold complexes, the absorption of at least four photons around 2350 cm⁻¹ is required to overcome the dissociation limit. The photon fluence generated from the table-top LaserVision system is insufficient to induce photofragmentation of [Cu(CO₂)₂]⁺ under the present experimental conditions. Consistent with this reasoning, we are not able to obtain significant photodissociation for the n = 2 cluster. Beginning at n = 3, the fragmentation can be observed. Higher fragmentation yield is obtained for n = 4–8. The number densities of n = 9–12 are insufficient for the obvious detection of laser-induced-dissociation fragmentation. Similar fragmentation feature holds true for the [Ag(CO₂)_n]⁺ (n = 1–12) clusters.

Alternatively, the technique of “messenger tagging” could be used to enhance the dissociation yield.^{9,29–32} Under the appropriate conditions (i.e., efficient cooling by supersonic expansion or cryogenic ion trap), the tagged complexes could be formed with weakly attached inert species that are transparent in the infrared (i.e., H₂, rare gas atoms), which are readily dissociated upon absorption of a single IR photon resonant because of low binding energy of “the messenger”. Unfortunately, it is difficult to generate sufficient tagged-[M(CO₂)_n]⁺ (M = Cu, Ag) complexes for the photodissociation measurement, which might be due to the warm source under the present experimental conditions.

4.1. [Cu(CO₂)_n]⁺. The experimental IRPD spectra of [Cu(CO₂)_n]⁺ (n = 3–8) are shown in Figure 2. The principal feature in the [Cu(CO₂)_n]⁺ (n = 3–8) complexes is observed at

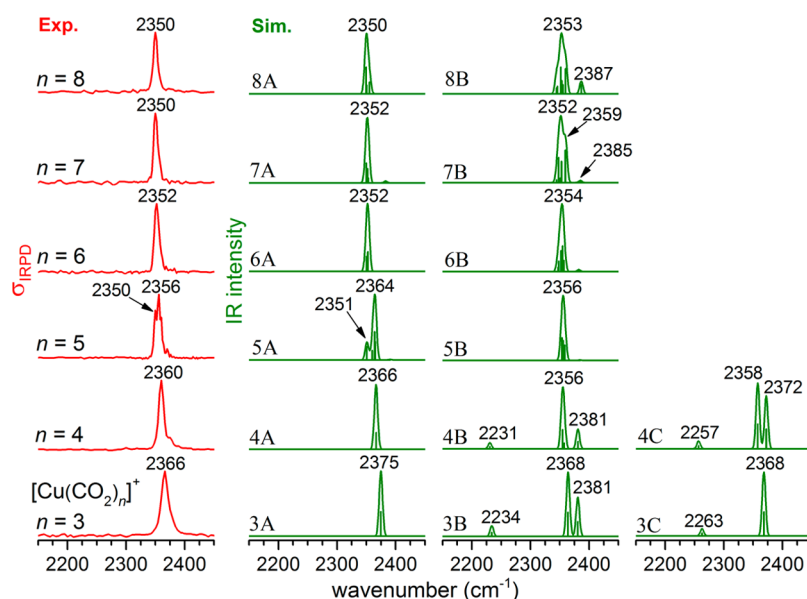


Figure 2. Experimental IRPD spectra (left column) and simulated harmonic IR spectra (right columns) in the CO_2 asymmetric stretch region of $[\text{Cu}(\text{CO}_2)_n]^+$ ($n = 3-8$).

2366, 2360, 2356, 2352, 2350, and 2350 cm^{-1} , respectively. These band positions are characteristic of the antisymmetric stretch of CO_2 .

The lowest-energy isomer of the $[\text{Cu}(\text{CO}_2)_3]^+$ cluster, labeled 3A, is a D_{3h} structure with a $^1A_1'$ ground state (Figure 3) in which the three CO_2 molecules are terminally bonded to the Cu cation in an end-on linear configuration (i.e., a so-called “3 + 0” species). [Note on the nomenclature: Using $i + j$, i denotes the number of CO_2 molecules in the first coordination shell, and j denotes the number of CO_2 molecules in the second coordination shell.] The 3A structure with a 3A_1 triplet state is 352.02 kJ/mol higher in energy. The next energetically higher isomer (3B, + 387.25 kJ/mol) involves a $[\text{OCuCO}(\text{CO}_2)_2]^+$ oxide-carbonyl structure. The 3C isomer consists of a bidentate double oxygen metal– CO_3 , a terminal CO, and an end-on CO_2 , which lies 419.11 kJ/mol higher in energy than 3A. The antisymmetric stretching vibrational frequencies of the CO_2 units in the 3A isomer are predicted to be 2375 cm^{-1} (Figure 2), which is consistent with the experimental value of 2366 cm^{-1} . In the simulated IR spectrum of isomer 3B, the band at 2234 cm^{-1} is attributed to the C–O stretch, which is not seen experimentally. The bands at 2368 and 2381 cm^{-1} are due to the CO_2 antisymmetric stretches of which the obvious splitting is absent from the experimental spectrum. For 3C, the simulated frequencies at 2263 and 2368 cm^{-1} are assigned to the C–O stretch and CO_2 antisymmetric stretch, respectively, of which the former is also not observed in the experiment. Furthermore, the isomers 3B and 3C (+387.25 and +419.11 kJ/mol) should be too high in energy to be probed in the experiment. Then, isomer 3A is responsible for the experimental IRPD spectrum of $[\text{Cu}(\text{CO}_2)_3]^+$ instead of 3B and 3C.

For $[\text{Cu}(\text{CO}_2)_4]^+$, the lowest-energy isomer (4A) has four terminally bonded CO_2 molecules with a C_{3v} symmetry and a 1A_1 ground state (Figure 3). The $[\text{OCuCO}(\text{CO}_2)_3]^+$ oxide-carbonyl structure (4B) lies 395.92 kJ/mol higher in energy than 4A. The 4C isomer consists of a $[(\text{OC})\text{Cu}(\text{CO}_3)(\text{CO}_2)_2]^+$ carbonyl-carbonate structure, which lies +414.21 kJ/mol above 4A. It can be seen from Figure 2 that the

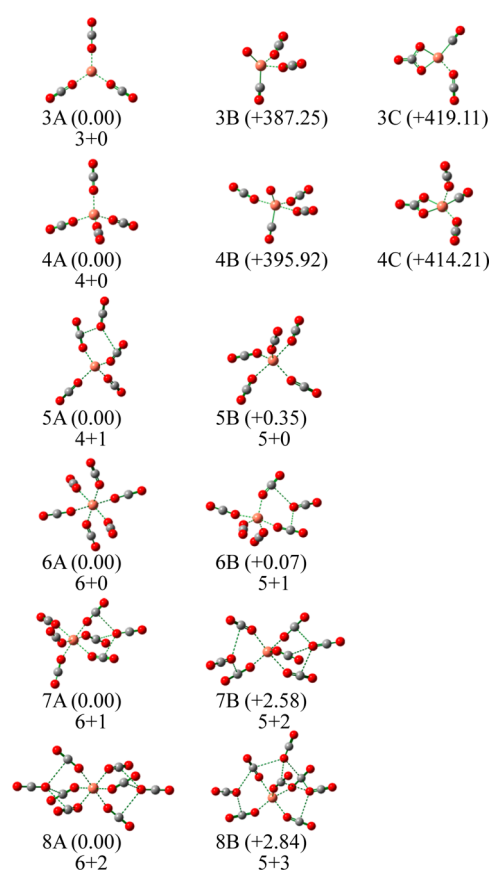


Figure 3. Optimized structures of $[\text{Cu}(\text{CO}_2)_n]^+$ ($n = 3-8$) (Cu, brown; C, gray; O, red). Relative energies (with ZPE correction) are given in kJ/mol.

simulated harmonic IR spectrum of 4A agrees best with experiment. In the simulated IR spectra of isomers 4B and 4C, the C–O stretches do not present in the experiment, as well as the splitting feature of CO_2 antisymmetric stretches. It thus appears that isomers 4B and 4C do not contribute to the

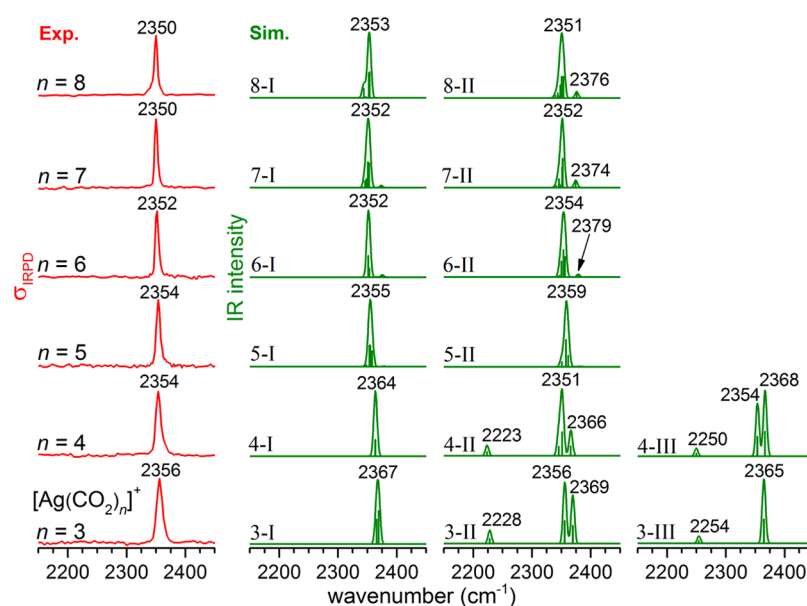


Figure 4. Experimental IRPD spectra (left column) and simulated harmonic IR spectra (right columns) in the CO_2 asymmetric stretch region of $[\text{Ag}(\text{CO}_2)_n]^+$ ($n = 3-8$).

experimental spectrum. Then, the $[\text{OCuCO}(\text{CO}_2)_{n-1}]^+$ oxide-carbonyl and $[(\text{OC})\text{Cu}(\text{CO}_3)(\text{CO}_2)_{n-2}]^+$ carbonyl-carbonate structures are not considered for the $n = 5-8$ clusters.

We have calculated the structures and harmonic IR spectra for $[\text{Cu}(\text{CO}_2)_5]^+$ with five ligands coordinated directly to the metal. The IR spectrum and structure of this five-coordinated species (isomer 5B) is shown in Figures 2 and 3, respectively. The 5B isomer yields a single strong peak at 2356 cm^{-1} , which reproduces the experiment. But there is no resonance for the shoulder peak of 2350 cm^{-1} observed experimentally. Alternatively, a structure with one external CO_2 (i.e., “4 + 1” configuration), labeled 5A in Figure 3, is predicted to be nearly energetically identical with 5B (i.e., “5 + 0” configuration). The 5A isomer yields two peaks at 2351 and 2364 cm^{-1} , which matches the experimental feature at 2350 and 2356 cm^{-1} . The vibrational mode at 2351 cm^{-1} in 5A is due to the CO_2 antisymmetric stretches of the second coordination shell. The barrier for the isomerization from 5A to 5B is calculated to be 6.96 kJ/mol , implying that the second shell CO_2 could easily move into the first shell and then move back. This indicates that the coexistence of isomers 5A and 5B is likely here.

As shown in Figure 3, the 6 + 0 and 5 + 1 structures for the $n = 6$ cluster are also comparable energetically and the calculated spectra of both isomers are consistent with the experiment (Figure 2). Hence, isomers 6A and 6B are responsible for $n = 6$. For $[\text{Cu}(\text{CO}_2)_7]^+$, the lowest-energy isomer (7A) has the 6 + 1 structure (Figure 3). The 5 + 2 structure (7B) is predicted to be $+2.58 \text{ kJ/mol}$ higher in energy above 7A. The calculated IR spectrum of 7A gives an intense peak at 2352 cm^{-1} , which reproduces well the experimental feature. The 7B isomer yields a broader band centered at 2352 cm^{-1} with a shoulder peak at 2359 cm^{-1} , which is discrepant from the experiment. The 7A isomer should be dominated in the $n = 7$ cluster. For $[\text{Cu}(\text{CO}_2)_8]^+$, the 6 + 2 structure (8A) is calculated to be more stable than the 5 + 3 structure (8B) by 2.84 kJ/mol (Figure 3). A single strong absorption is observed at 2350 cm^{-1} in the simulated IR spectrum of 8A (Figure 2), which nicely reproduces the experiment. In contrast, the 8B isomer yields two peaks at 2353 and 2387 cm^{-1} , whereas the latter is absent

from the experiment. The 8A isomer should be responsible for the experimental spectrum of $n = 8$.

4.2. $[\text{Ag}(\text{CO}_2)_n]^+$. The comparison of the experimental IRPD spectra to the simulated harmonic IR spectra of $[\text{Ag}(\text{CO}_2)_n]^+$ ($n = 3-8$) is given in Figure 4 and the optimized structures of the corresponding isomers are shown in Figure 5. Experimentally, the principal band in $[\text{Ag}(\text{CO}_2)_n]^+$ ($n = 3-8$) appears at 2356 , 2354 , 2354 , 2352 , 2350 , and 2350 cm^{-1} , respectively. The lowest-energy isomer of $[\text{Ag}(\text{CO}_2)_3]^+$ (3-I) is a 3 + 0 structure with a $^1\text{A}_1$ ground state (Figure 5). The 3-II and 3-III isomers consist of oxide-carbonyl and carbonyl-carbonate structure, respectively. The CO_2 antisymmetric stretching vibrational frequencies in 3-I are calculated to be 2367 cm^{-1} (Figure 4), which is consistent with the experimental value of 2356 cm^{-1} . Similar to the $[\text{Cu}(\text{CO}_2)_3]^+$ cluster, the presence of isomers 3-II and 3-III can be eliminated on the basis of the C–O stretches that are not observed experimentally. For the $[\text{Ag}(\text{CO}_2)_4]^+$ cluster, the lowest-lying isomer is predicted to be a 4 + 0 structure with a $^1\text{A}_1$ ground state (4-I) (Figure 5). The oxide-carbonyl (4-II) and carbonyl-carbonate (4-III) structures lie 459.89 and 495.19 kJ/mol higher in energy above 4-I, respectively. The simulated IR spectrum of 4-I agrees best with experiment. Isomers 4-II and 4-III can be ruled out on the basis of the absence of the C–O stretches and the splitting feature of CO_2 antisymmetric stretches from the experiment.

For $[\text{Ag}(\text{CO}_2)_5]^+$, the lowest-energy isomer (5-I) has a five-coordinated structure (Figure 5). The 4 + 1 structure (5-II) lies 3.63 kJ/mol higher in energy than 5-I. As shown in Figure 4, the simulated harmonic IR spectrum of 5-I is similar to that of 5-II, both of which agrees with experiment. It thus appears that the coexistence of isomers 5-I and 5-II is likely for $[\text{Ag}(\text{CO}_2)_5]^+$. Analogously, the coexistence of isomers 6-I and 6-II is also likely for $[\text{Ag}(\text{CO}_2)_6]^+$. For $[\text{Ag}(\text{CO}_2)_{n=7,8}]^+$, the lowest-energy isomers (7-I and 8-I) consist of the $n + 0$ configuration (Figure 5). The $(n - 1) + 1$ structure is predicted to be less stable by 2.15 and 3.38 kJ/mol for $n = 7$ and 8 , respectively. The $n + 0$ structure yields the strong absorption at 2352 and 2353 cm^{-1} for $n = 7$ and 8 (Figure 4), respectively,

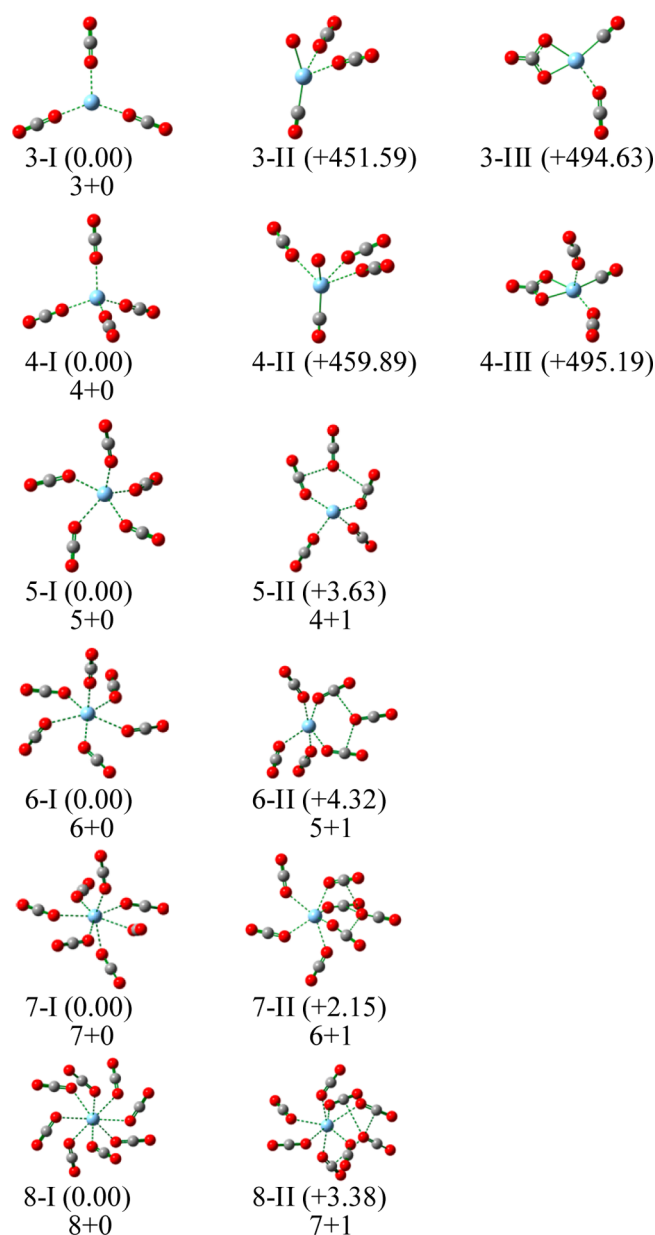


Figure 5. Optimized structures of $[\text{Ag}(\text{CO}_2)_n]^+$ ($n = 3-8$) (Ag, light cyan; C, gray; O, red). Relative energies (with ZPE correction) are given in kJ/mol.

which is consistent with the experiment. Besides this principal band of CO_2 antisymmetric stretch, satellite peak appears at 2374 and 2376 cm^{-1} for $n = 7$ and 8 in the $(n - 1) + 1$ structure, respectively, in which the intensity increases with the increase of cluster size. However, this new feature is not observed in the experiment. The $n + 0$ structure should be dominated in the $[\text{Ag}(\text{CO}_2)_{n=7,8}]^+$ clusters.

4.3. Structural Evolution of the $[\text{M}(\text{CO}_2)_n]^+$ ($\text{M} = \text{Cu}, \text{Ag}$) Complexes. The agreement between the experimental and theoretical results allows for establishing the structural evolution of $[\text{M}(\text{CO}_2)_n]^+$ ($\text{M} = \text{Cu}, \text{Ag}; n = 3-8$). The blueshift of antisymmetric stretch of CO_2 in $[\text{M}(\text{CO}_2)_n]^+$ from the free CO_2 molecule at 2349 cm^{-1} is plotted as a function of cluster size in Figure 6. The core vibrational band in $[\text{Cu}(\text{CO}_2)_n]^+$ ($n = 3-8$) is blue-shifted by 17, 11, 7, 3, 1, and 1 cm^{-1} , respectively. For $[\text{Ag}(\text{CO}_2)_n]^+$ ($n = 3-8$), the blueshift is 7, 5, 5, 3, 1, and 1 cm^{-1} , respectively. Then, the

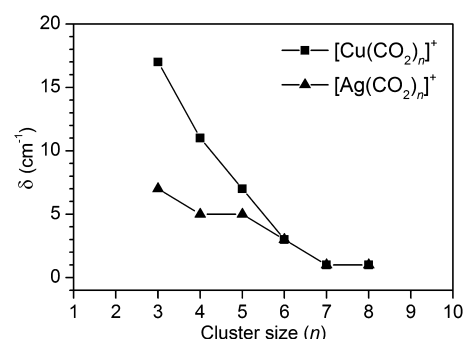


Figure 6. Plot of the core vibrational band as a function of cluster size. The shift (δ) for the antisymmetric stretch of CO_2 in $[\text{M}(\text{CO}_2)_n]^+$ ($\text{M} = \text{Cu}, \text{Ag}$) is compared to that in the free- CO_2 molecule at 2349 cm^{-1} .

blueshift in $[\text{M}(\text{CO}_2)_n]^+$ ($\text{M} = \text{Cu}, \text{Ag}; n = 3-8$) decreases with the increase of cluster size. As illustrated in Figure 6, the converged trend of such blueshift indicates the coordination of the Cu^+ and Ag^+ cations with CO_2 tends to be saturated around $n = 7-8$.

For $[\text{M}(\text{CO}_2)_3]^+$ ($\text{M} = \text{Cu}, \text{Ag}$), the 3 + 0 structure is favored (Figures 3 and 5), which includes a three-coordinated configuration. Similarly, the 4 + 0 structure is found to be responsible for the $n = 4$ cluster. The formation of oxide-carbonyl and carbonyl-carbonate structures is not favored for the interaction of CO_2 with Cu^+ and Ag^+ . For $[\text{M}(\text{CO}_2)_5]^+$ ($\text{M} = \text{Cu}, \text{Ag}$), the two nearly energy-identical 5 + 0 and 4 + 1 structures coexist in the present experiment. Then, the $n = 5$ spectrum does not require all of the complexes this size to have such a 5 + 0 configuration. This behavior is similar to the clustering of H_2O or acetylene around Ni^+ , but quite different from the clustering of CO_2 around Ni^+ . The 6 + 0 and 5 + 1 structures are assigned to be the structures for $n = 6$. While the six-coordinated structure is favored for $[\text{Cu}(\text{CO}_2)_{n=7,8}]^+$, the $n + 0$ configuration is dominated for $[\text{Ag}(\text{CO}_2)_{n=7,8}]^+$. The maximum number of CO_2 in the first shell for Cu^+ and Ag^+ seems to be 6 and 8, respectively. Such difference could be due to that the larger sized Ag^+ could accommodate more CO_2 ligands in the direct solvation shell (the effective ion radius of Cu^+ and Ag^+ is 0.91 and 1.29 Å, respectively).³³ It can be found from the lowest-lying isomers that the second coordination shell starts to appear in the $n \geq 5$ clusters of $[\text{Cu}(\text{CO}_2)_n]^+$, whereas that is reluctant to present in $[\text{Ag}(\text{CO}_2)_n]^+$. This could be due to the smaller repulsion between CO_2 in the first coordination shell of Ag^+ because of its larger ion radius.

4.4. Comparison of the $\text{Cu}^+/\text{Ag}^+ + \text{CO}_2$ Coordination with Different Metal and Different Charge State.

Summarizing, the Cu^+ and Ag^+ cations bind to an oxygen atom of CO_2 in an end-on configuration via a charge-quadrupole electrostatic interaction in the $[\text{M}(\text{CO}_2)_n]^+$ complexes studied here. The asymmetric stretch motion of CO_2 experiences greater repulsion on its inner turning point, and the corresponding vibrational band shifts to higher frequency than those in the isolated molecule, accounting for the blueshifts of CO_2 antisymmetric stretching vibrational frequencies. Similar blue-shifted bands for the CO_2 ligands attached directly to the metal have also been observed for Mg^+ , Al^+ , Si^+ , V^+ , Fe^+ , and Ni^+ .^{13,14,16,26,27,34,35} In contrast, the oxide-carbonyl structure has been found for Ti^+ .¹⁵ A carbonyl-carbonate structure has been observed for molybdenum in the $\text{Mo}_4(\mu_4-\text{CO}_3)(\text{CO})_2(\text{O})_2(\mu_2-\text{O})_2(\mu_2-\text{OH})_4(\text{PMe}_3)_6$ complex derived from the metal-induced reductive disproportionation of

carbon dioxide.³⁶ Matrix-isolation infrared spectroscopic studies reveal that the early lanthanoid (La–Sm) oxocarbonyl complexes adopt the trans-configurations, the europium and ytterbium ones adopt side-on-bonded modes (Eu-(η^2 -OC)O and Yb-(η^2 -OC)O), and the late lanthanoid (Gd–Lu) ones adopt the cis-configurations.³⁷ Interestingly, recent infrared photodissociation spectroscopic study of $[V(\text{CO}_2)_n]^+$ allows identification of an oxalate-type C_2O_4 anion species at $n = 7$.¹⁶ This suggests that there is a solvent-driven intracluster reaction resulting in the formation of a V^{2+} metal ion and a C_2O_4^- anion. The activation of CO_2 producing this novel species occurs via a metal-to-ligand electron transfer reaction, which is driven by a combination of the creation of an expanded coordination sphere around the V^{2+} dication, electrostatic attraction between the hexa-coordinated dication and the nascent C_2O_4^- anion, and the solvation energy of the two ionic species. Monodentate structure $[M(\eta^1\text{-CO}_2)]^-$ is favored for Cu^- , Ag^- , Au^- , and Bi^- anions^{17–20} and bidentate configuration $[M(\eta^2\text{-CO}_2)]^-$ for Co^- and Ni^- .^{21,22} Especially, the transition of metalloformate to oxalate complexes has been evidenced for Bi^- with the increase of cluster size, revealing the reductive activation of a CO_2 ligand by a single-atom catalyst.²⁰ These investigations would have important implications for understanding the interaction of CO_2 with reduction catalysts and rationally designing catalysts for CO_2 reduction based on cost-effective transition metals.

5. CONCLUSIONS

The approach of infrared photodissociation spectroscopy combined with quantum chemical calculation was employed to probe the reaction of copper and silver cations with carbon dioxide. The $[M(\text{CO}_2)_n]^+$ ($M = \text{Cu}, \text{Ag}$) cations were generated via a laser vaporization supersonic cluster source in the gas phase and mass selected to interact with infrared laser. The Cu^+ and Ag^+ cations bind to an oxygen atom of CO_2 in an end-on configuration via a charge-quadrupole electrostatic interaction. The formation of oxide-carbonyl and carbonyl-carbonate structures is not evidenced in the reaction of CO_2 with Cu^+ and Ag^+ . For $n = 3$ and 4, the $n + 0$ structure is preferred. The two nearly energy-identical $n + 0$ and $(n - 1) + 1$ structures coexist in $n = 5$ and 6. While the six-coordinated structure is favored for $[\text{Cu}(\text{CO}_2)_{n=7,8}]^+$, the $n + 0$ configuration is dominated in $[\text{Ag}(\text{CO}_2)_{n=7,8}]^+$. The reaction of CO_2 with the cationic metal atoms has been compared to that with the neutral and anionic metal atoms, which would have important implications for understanding and rationally designing CO_2 activation and reduction based on cost-effective transition metals.

■ ASSOCIATED CONTENT

Supporting Information

The Supporting Information is available free of charge on the ACS Publications website at DOI: 10.1021/acs.jpca.7b01320.

Mass spectrum of $[\text{Ag}(\text{CO}_2)_n]^+$ (Figure S1) (PDF)

■ AUTHOR INFORMATION

Corresponding Author

*E-mail: ljiang@dicp.ac.cn. Tel.: +86-411-84379857. Fax: +86-411-84675584.

ORCID

Jijun Zhao: 0000-0002-3263-7159

Ling Jiang: 0000-0002-8485-8893

Author Contributions

||Z.Z. and X.K. contributed equally to this work.

Notes

The authors declare no competing financial interest.

■ ACKNOWLEDGMENTS

This work was supported by the National Natural Science Foundation of China (Grants 21327901, 21503222, 21673231, and 11574040), the Key Research Program (Grant KGZD-EW-T05), and the Strategic Priority Research Program (Grant XDB17010000) of the Chinese Academy of Science. L.J. acknowledges the Hundred Talents Program of Chinese Academy of Sciences.

■ REFERENCES

- (1) Freund, H. J.; Roberts, M. W. Surface Chemistry of Carbon Dioxide. *Surf. Sci. Rep.* **1996**, *25*, 225–273.
- (2) Gibson, D. H. The Organometallic Chemistry of Carbon Dioxide. *Chem. Rev.* **1996**, *96*, 2063–2095.
- (3) Taifan, W.; Boily, J.-F.; Baltrusaitis, J. Surface Chemistry of Carbon Dioxide Revisited. *Surf. Sci. Rep.* **2016**, *71*, 595–671.
- (4) Castleman, A. W.; Keese, R. G. Clusters - Bridging the Gas and Condensed Phases. *Acc. Chem. Res.* **1986**, *19*, 413–419.
- (5) Bohme, D. K.; Schwarz, H. Gas-phase Catalysis by Atomic and Cluster Metal Ions: The Ultimate Single-site Catalysts. *Angew. Chem., Int. Ed.* **2005**, *44*, 2336–2354.
- (6) Freund, H. J.; Meijer, G.; Scheffler, M.; Schlogl, R.; Wolf, M. CO Oxidation as a Prototypical Reaction for Heterogeneous Processes. *Angew. Chem., Int. Ed.* **2011**, *50*, 10064–10094.
- (7) Luo, Z.; Castleman, A. W., Jr.; Khanna, S. N. Reactivity of Metal Clusters. *Chem. Rev.* **2016**, *116*, 14456–14492.
- (8) Mascetti, J.; Galan, F.; Papai, I. Carbon Dioxide Interaction with Metal Atoms: Matrix Isolation Spectroscopic Study and DFT Calculations. *Coord. Chem. Rev.* **1999**, *190–192*, 557–576.
- (9) Walker, N. R.; Walters, R. S.; Duncan, M. A. Frontiers in the Infrared Spectroscopy of Gas Phase Metal Ion Complexes. *New J. Chem.* **2005**, *29*, 1495–1503.
- (10) Weber, J. M. The Interaction of Negative Charge with Carbon Dioxide - Insight into Solvation, Speciation and Reductive Activation from Cluster Studies. *Int. Rev. Phys. Chem.* **2014**, *33*, 489–519.
- (11) Zhou, M. F.; Andrews, L. Infrared Spectra and Density Functional Calculations for OscCO , $\text{Sc}(\eta^2\text{-OC})\text{O}$, $\text{Osc}(\eta^2\text{-CO})$, and Three OscCO^+ Cation Isomers in Solid Argon. *J. Am. Chem. Soc.* **1998**, *120*, 13230–13239.
- (12) Jiang, L.; Teng, Y.-L.; Xu, Q. Infrared Spectroscopic and Density Functional Theory Study on the Reactions of Rhodium and Cobalt Atoms with Carbon Dioxide in Rare-gas Matrixes. *J. Phys. Chem. A* **2007**, *111*, 7793–7799.
- (13) Jaeger, J. B.; Jaeger, T. D.; Brinkmann, N. R.; Schaefer, H. F.; Duncan, M. A. Infrared Photodissociation Spectroscopy of $\text{Si}^+(\text{CO}_2)_n$ and $\text{Si}^+(\text{CO}_2)_n\text{Ar}$ Complexes - Evidence for Unanticipated Intracluster Reactions. *Can. J. Chem.* **2004**, *82*, 934–946.
- (14) Walker, N. R.; Walters, R. S.; Duncan, M. A. Infrared Photodissociation Spectroscopy of $\text{V}^+(\text{CO}_2)_n$ and $\text{V}^+(\text{CO}_2)_n\text{Ar}$ Complexes. *J. Chem. Phys.* **2004**, *120*, 10037–10045.
- (15) Xing, X.-P.; Wang, G.-J.; Wang, C.-X.; Zhou, M.-F. Infrared Photodissociation Spectroscopy of $\text{Ti}^+(\text{CO}_2)_2\text{Ar}$ and $\text{Ti}^+(\text{CO}_2)_n$ ($n = 3–7$) Complexes. *Chin. J. Chem. Phys.* **2013**, *26*, 687–693.
- (16) Ricks, A. M.; Brathwaite, A. D.; Duncan, M. A. IR Spectroscopy of Gas Phase $\text{V}(\text{CO}_2)_n^+$ Clusters: Solvation-Induced Electron Transfer and Activation of CO_2 . *J. Phys. Chem. A* **2013**, *117*, 11490–11498.
- (17) Knurr, B. J.; Weber, J. M. Solvent-Driven Reductive Activation of Carbon Dioxide by Gold Anions. *J. Am. Chem. Soc.* **2012**, *134*, 18804–18808.
- (18) Knurr, B. J.; Weber, J. M. Solvent-Mediated Reduction of Carbon Dioxide in Anionic Complexes with Silver Atoms. *J. Phys. Chem. A* **2013**, *117*, 10764–10771.

(19) Knurr, B. J.; Weber, J. M. Structural Diversity of Copper-CO₂ Complexes: Infrared Spectra and Structures of Cu(CO₂)_n⁻ Clusters. *J. Phys. Chem. A* **2014**, *118*, 10246–10251.

(20) Thompson, M. C.; Ramsay, J.; Weber, J. M. Solvent-Driven Reductive Activation of CO₂ by Bismuth: Switching from Metalloformate Complexes to Oxalate Products. *Angew. Chem., Int. Ed.* **2016**, *55*, 15171–15174.

(21) Knurr, B. J.; Weber, J. M. Infrared Spectra and Structures of Anionic Complexes of Cobalt with Carbon Dioxide Ligands. *J. Phys. Chem. A* **2014**, *118*, 4056–4062.

(22) Knurr, B. J.; Weber, J. M. Interaction of Nickel with Carbon Dioxide in Ni(CO₂)_n⁻ Clusters Studied by Infrared Spectroscopy. *J. Phys. Chem. A* **2014**, *118*, 8753–8757.

(23) Miller, G. B. S.; Esser, T. K.; Knorke, H.; Gewinner, S.; Schoellkopf, W.; Heine, N.; Asmis, K. R.; Uggerud, E. Spectroscopic Identification of a Bidentate Binding Motif in the Anionic Magnesium-CO₂ Complex ([ClMgCO₂]⁻). *Angew. Chem., Int. Ed.* **2014**, *53*, 14407–14410.

(24) Xie, H.; Wang, J.; Qin, Z. B.; Shi, L.; Tang, Z. C.; Xing, X. P. Octacoordinate Metal Carbonyls of Lanthanum and Cerium: Experimental Observation and Theoretical Calculation. *J. Phys. Chem. A* **2014**, *118*, 9380–9385.

(25) Frisch, M. J.; et al. *Gaussian 09*; Gaussian, Inc.: Wallingford, CT, 2009.

(26) Gregoire, G.; Duncan, M. A. Infrared Spectroscopy to Probe Structure and Growth Dynamics in Fe⁺(CO₂)_n Clusters. *J. Chem. Phys.* **2002**, *117*, 2120–2130.

(27) Walker, N. R.; Walters, R. S.; Grieves, G. A.; Duncan, M. A. Growth Dynamics and Intracuster Reactions in Ni⁺(CO₂)_n Complexes via Infrared Spectroscopy. *J. Chem. Phys.* **2004**, *121*, 10498–10507.

(28) Iskra, A.; Gentleman, A. S.; Kartouzian, A.; Kent, M. J.; Sharp, A. P.; Mackenzie, S. R. Infrared Spectroscopy of Gas-Phase M⁺(CO₂)_n (M = Co, Rh, Ir) Ion–Molecule Complexes. *J. Phys. Chem. A* **2017**, *121*, 133–140.

(29) Okumura, M.; Yeh, L. I.; Lee, Y. T. The Vibrational Predissociation Spectroscopy of Hydrogen Cluster Ions. *J. Chem. Phys.* **1985**, *83*, 3705–3706.

(30) Okumura, M.; Yeh, L. I.; Lee, Y. T. Infrared Spectroscopy of the Cluster Ions H₃⁺(H₂)_n. *J. Chem. Phys.* **1988**, *88*, 79–91.

(31) Wang, G. J.; Zhou, M. F.; Goettel, J. T.; Schrobilgen, G. J.; Su, J.; Li, J.; Schloeder, T.; Riedel, S. Identification of an Iridium-containing Compound with a Formal Oxidation State of IX. *Nature* **2014**, *514*, 475–478.

(32) Heine, N.; Asmis, K. R. Cryogenic Ion Trap Vibrational Spectroscopy of Hydrogen-bonded Clusters Relevant to Atmospheric Chemistry. *Int. Rev. Phys. Chem.* **2015**, *34*, 1–34.

(33) Shannon, R. D. Revised Effective Ionic Radii and Systematic studies of Interatomic Distances in Halides and Chalcogenides. *Acta Crystallogr., Sect. A: Cryst. Phys., Diffraction, Theor. Gen. Crystallogr.* **1976**, *32*, 751–767.

(34) Gregoire, G.; Brinkmann, N. R.; van Heijnsbergen, D.; Schaefer, H. F.; Duncan, M. A. Infrared Photodissociation Spectroscopy of Mg⁺(CO₂)_n and Mg⁺(CO₂)_nAr Clusters. *J. Phys. Chem. A* **2003**, *107*, 218–227.

(35) Walters, R. S.; Brinkmann, N. R.; Schaefer, H. F.; Duncan, M. A. Infrared Photodissociation Spectroscopy of Mass-Selected Al⁺(CO₂)_n and Al⁺(CO₂)_nAr Clusters. *J. Phys. Chem. A* **2003**, *107*, 7396–7405.

(36) Alvarez, R.; Atwood, J. L.; Carmona, E.; Perez, P. J.; Poveda, M. L.; Rogers, R. D. Formation of Carbonyl Carbonate Complexes of Molybdenum by Reductive Disproportionation of Carbon Dioxide. *Inorg. Chem.* **1991**, *30*, 1493–1499.

(37) Jiang, L.; Zhang, X.-B.; Han, S.; Xu, Q. Unique Structural Trends in the Lanthanoid Oxocarbonyl Complexes. *Inorg. Chem.* **2008**, *47*, 4826–4831.